Proton Bernstein instability in the magnetosphere: Linear dispersion theory

S. Peter Gary, Kaijun Liu, and Dan Winske

Los Alamos National Laboratory, Los Alamos, New Mexico

S. Peter Gary, Kaijun Liu, and Dan Winske, Los Alamos National Laboratory, Los Alamos, NM 87545. (e-mail: pgary@lanl.gov, kaijun@lanl.gov, winske@lanl.gov)

Abstract. Kinetic linear dispersion theory for electromagnetic fluctuations in a homogeneous collisionless plasma is used to study the properties of a proton Bernstein mode instability driven by a proton velocity distribution $f_p(\mathbf{v})$ such that $\partial f_p(v_\perp)/\partial v_\perp > 0$ at suprathermal values of $v_\perp$ where $||$ and $\perp$ denote directions parallel and perpendicular to the background magnetic field $\mathbf{B}_o$, respectively. The model uses a three-component proton velocity distribution with $f_p(\mathbf{v}) = f_1(v) + f_2(v_{||}, v_\perp) - f_3(v_{||}, v_\perp)$ where $f_1(v)$ represents a Maxwellian thermal component. Here f_2 and f_3 are bi-Maxwellians with $T_{\perp p} > T_{||p}$ and slightly different densities and temperatures to represent a suprathermal velocity ring component consistent with nonthermal proton perpendicular velocity distributions observed in the magnetospheric ring current. As is well established, the growth rate of the resulting instability has relative maxima at harmonics of the proton cyclotron frequency, the wavevector $\mathbf{k}$ satisfies $0 < \quad k_{||} \quad << \quad k_\perp$ and wavelengths are of the order of or smaller than the proton gyroradius. The instability growth rate decreases as the electron/thermal-proton temperature ratio increases and, for the dimensionless parameters chosen here, has a maximum value for the thermal proton β of about 10%.

1. Introduction

Enhanced magnetic and electric field fluctuations at frequencies between the proton cyclotron frequency and the lower hybrid frequency and at propagation nearly perpendicular to $\mathbf{B}_o$ are observed frequently near the equatorial plane of the terrestrial magnetosphere. Such enhanced fluctuations were first called "equatorial noise" [*Russell et al.*, 1970; *Santolík et al.*, 2002, 2004], but more recently have been termed "magnetosonic waves" [*Perraut et al.*, 1982; *Pokhotelov et al.*, 2008]. *Horne et al.* [2007] suggested that these enhanced fluctuations may accelerate electrons from tens of keV up to a few MeV in the outer radiation belt. This has stimulated substantial recent interest in these fluctuations [*Meredith et al.*, 2008, 2009; *Tao et al.*, 2009; *Shprits*, 2009; *Ni and Summers*, 2010; *Bortnik and Thorne*, 2010]. Magnetospheric observations characterize the unstable proton velocity distributions $f_p(\mathbf{v})$ associated with these "magnetosonic waves" as having a velocity-ring type property or, more generally, with $\partial f_p(v_\perp)/\partial v_\perp > 0$ where $\perp$ denotes directions perpendicular to the background magnetic field $\mathbf{B}_o$ [*Perraut et al.*, 1982; *Boardsen et al.*, 1992; *Meredith et al.*, 2008; *Borovsky and Denton*, 2009; *Denton et al.*, 2010]. Such unstable proton velocity distributions have also been obtained from the RAM magnetospheric model [*Jordanova et al.*, 1997]. *Chen et al.* [2010] used the RAM model to show that, as a result of injection during magnetic storms, proton velocity distributions $f_p(\mathbf{v})$ near midnight are essentially bi-Maxwellian with $T_\perp/T_\parallel > 1$, where the subscripts indicate directions relative to the background magnetic field $\mathbf{B}_o$. But between prenoon and duskside, energy-dependent ion convection leads to a velocity-ring distributions with the property $\partial f_p(v_\perp)/\partial v_\perp > 0$ at suprathermal perpendicular velocities. *Chen* *et al.* [2011] analyzed energetic proton measurements from geosynchronous orbit during the April 2001 magnetic storm to show that proton velocity rings can form over a broad spatial region from noon to pre-midnight. Furthermore, these authors used the approximate linear theory of *Chen et al.* [2010] and the observed proton velocity distributions to calculate convective growth rates of the resulting instability.

If the positive slope of $f_p(v_\perp)$ is sufficiently steep, kinetic linear dispersion theory in a relatively homogeneous, collisionless, magnetized plasma predicts that electromagnetic proton Bernstein modes at $0 < k_{||} << k_\perp$ become unstable at harmonics of the proton cyclotron frequency. *Perraut et al.* [1982] considered a cold plasma with a cold proton velocity ring to show that, at $k_{||} = 0$, a proton-driven instability would be excited near crossings between the magnetosonic/whistler wave and the various Bernstein mode harmonics. In this cold plasma approximation, the two critical parameters are the relative density of the ring and the relative ring speed. The growth rate becomes stronger for increasing ion ring densities, and, for the relatively weak ring components typical to the magnetosphere, the instability is excited only when the perpendicular ring speed is larger than the Alfvén speed. Further studies considered thermal electron and ion components [*Boardsen et al.*, 1992; *McClements and Dendy*, 1993; *Horne et al.*, 2000]; for example, *McClements et al.* [1994] showed that thermal effects allow the cyclotron harmonic instability to grow at propagation angles out to at least 10^o from directions strictly perpendicular to $\mathbf{B}_o$. *Akimoto et al.* [1985] showed that the growth rate is quite sensitive to the electron temperature and decreases with increasing T_e/T_p.

Some particle-in-cell simulations have addressed the nonlinear consequences of this instability in the electrostatic limit [e.g., *Lee and Birdsall*, 1979; *Roth and Hudson*, 1985;

Janhunen et al., 2003; *Ashour-Abdalla et al.*, 2006]. But few simulations have addressed the fully electromagnetic properties of this instability [*Lee and Birdsall*, 1979] in the non-zero-β regime appropriate for the terrestrial magnetosphere. Recently *Liu et al.* [2011] have carried out fully electromagnetic particle-in-cell simulations of the proton Berstein instability. The simulation results agree well with a kinetic linear dispersion analysis and demonstrate that proton scattering by the enhanced fluctuations is a prime cause for the reduction of the $\partial f_p(v_\perp)/\partial v_\perp > 0$ and the consequent saturation of instability growth.

Here we solve the full kinetic linear dispersion equation for the proton Bernstein instability driven by $\partial f_p(v_\perp)/\partial v_\perp > 0$ at suprathermal speeds in a homogeneous, collisionless, magnetized plasma. We derive scaling relations for the growth rate of this instability as a function of the thermal proton β and the electron/thermal-proton temperature ratio.

The term "magnetosonic waves" has been incorrectly applied to fluctuations observed in the magnetosphere. In magnetohydrodynamic (MHD) theory, magnetosonic waves correspond to the normal mode which, at propagation oblique to the background magnetic field, is compressive and has a phase speed faster than the incompressible Alfven mode. Because MHD theory is limited to frequencies much below the proton cyclotron frequency, magnetosonic waves have historically been associated with such very low frequencies. Unfortunately, many observers have applied the "magnetosonic" label to their measurements of compressional modes above the proton cyclotron frequency. We will bow to precedent and use this incorrect term in referring to magnetospheric observations. But we insist on using the more appropriate term "proton Bernstein mode instability" (omitting "mode" for the sake of brevity) in describing linear theory calculations of the growing fluctuations studied here.

We denote the jth species plasma frequency as $\omega_j \equiv \sqrt{4\pi n_o e^2/m_j}$, the jth species cyclotron frequency as $\Omega_j \equiv e_j B_o/m_j c$, the jth component thermal speed as $v_j \equiv \sqrt{k_B T_{\parallel j}/m_j}$, and $\tilde{\beta}_j \equiv 8\pi n_o k_B T_j/B_o^2$. The Alfvén speed is $v_A \equiv B_o/\sqrt{4\pi n_o m_i}$. Here n_o is the total plasma density, $\mathbf{B}_o$ denotes the uniform background magnetic field, and we consider a two-species plasma of electrons (subscript e) and protons (subscript p). The complex frequency $\omega = \omega_r + i\gamma$ where $\gamma > 0$ indicates a growing fluctuation. We define the magnetic compressibility as

$$C_\parallel \equiv \frac{|\delta B_\parallel|^2}{|\delta \mathbf{B}|^2} \tag{1}$$

[*Gary et al.*, 2010] and the electric/magnetic field energy ratio as

$$\sigma_{EE} \equiv \frac{|\delta \mathbf{E}|^2}{|\delta \mathbf{B}|^2} \tag{2}$$

[*Gary*, 1993, Eq. (5.2.5)].

Although the subscript $\perp$ generally indicates a direction perpendicular to $\mathbf{B}_o$, we warn the reader that it is applied in two different contexts here. We use $v_\perp$ in the usual sense, that is, to denote the magnitude of the perpendicular velocity in cylindrical coordinates. However, for vector quantities associated with spatial variations, including $\mathbf{k}$, $\delta\mathbf{B}$, and $\delta\mathbf{E}$, we use $\perp$ to denote one of the two perpendicular coordinates. The Cartesian coordinate system of our linear dispersion theory [*Gary*, 1993] admits spatial variations in both the direction parallel to $\mathbf{B}_o$ (denoted by $||$) and one direction perpendicular to the background field (denoted by $\perp$), but no spatial variations in the other perpendicular direction (denoted by $\perp\perp$). So the real wavevector is defined as $\mathbf{k} \equiv \hat{\mathbf{z}}k_\parallel + \hat{\mathbf{y}}k_\perp = \hat{\mathbf{z}}k\cos\theta + \hat{\mathbf{y}}k\sin\theta$ where θ denotes the wavevector direction relative to $\mathbf{B}_o$.

2. Linear Theory

This section describes our numerical solutions for the properties of the proton Bernstein instability driven by $\partial f_p(v_\perp)/\partial v_\perp > 0$ at suprathermal perpendicular speeds using the linear dispersion equation for electromagnetic fluctuations in a homogeneous, magnetized, collisionless plasma. Under the assumption that the plasma species velocity distributions can be represented as the sum of several Maxwellians or bi-Maxwellians, the analytic form for this dispersion equation is given, for example, by *Stix* [1992] and *Gary* [1993]. In contrast to several of the approximate linear theory analyses cited above, we here, as *Denton et al.* [2010] and *Gary et al.* [2010], numerically solve the full dispersion equation for thermal proton and electron velocity distributions for arbitrary angles of propagation relative to $\mathbf{B}_o$.

Denton et al. [2010] and *Gary et al.* [2010] examined linear theory solutions for proton velocity distributions as observed in the plasma sheet boundary layer. Such distributions have positive slopes in $v_\perp$ at speeds relatively small compared to the overall proton thermal speed, and may be represented as the difference of two Maxwellians. In contrast here our concern is instability growth in the magnetospheric ring current, where both observations [*Perraut et al.*, 1982; *Boardsen et al.*, 1992; *Meredith et al.*, 2008; *Borovsky and Denton*, 2009; *Chen et al.*, 2011] and ring current models [*Chen et al.*, 2010] show that stormtime proton velocity distributions may consist of a relatively cool, relatively dense, relatively isotropic thermal component and a relatively hot, relatively tenuous, velocity-ring-like part. In this case the regime of $\partial f_p(v_\perp)/\partial v_\perp > 0$ arises at $v_\perp$ values greater than the average speed of the thermal component. To represent such a case, we here consider proton velocity distributions constructed from three components in the form

$$f_p(\mathbf{v}) = f_1(v) + f_2(v_{\|}, v_{\perp}) - f_3(v_{\|}, v_{\perp})$$

where each component is a bi-Maxwellian with

$$f_j(v_{\|}, v_{\perp}) = \frac{n_j}{(2\pi v_j^2)^{3/2}} \frac{T_{\|j}}{T_{\perp j}} \exp(-v_{\|}^2/2v_j^2) \exp(-v_{\perp}^2 T_{\|j}/2v_j^2 T_{\perp j})$$

Here f_1 is the thermal proton component represented by an isotropic Maxwellian distribution with $T_{\|1} = T_{\perp 1}$. Thus, using the definitions of Section 1, $v_1^2/v_A^2 = \tilde{\beta}_1/2$. The two other components are hotter and anisotropic with $T_{\perp j}/T_{\|j} > 1$ so that their difference represents a velocity-ring-like distribution with positive slope in the perpendicular velocity distribution. We call this the "three-component" proton model. Note that because we do not include a dense, cold ion component, this model is less appropriate to represent proton distributions in the plasmasphere, but is more relevant for protons in the outer magnetosphere [*Perraut et al.*, 1982; *Meredith et al.*, 2008]. We define $n_o \equiv n_1 + n_2 - n_3$ and $n_o T_p \equiv n_1 T_1 + n_2 T_2 - n_3 T_3$. The electrons are described by a single Maxwellian velocity distribution.

The ring current observations and models cited above demonstrate a broad range of parameters for unstable proton velocity ring distributions. The numerical algorithm of our dispersion solver uses an increasing number of Bessel functions to compute dispersion at increasing values of ω_r/Ω_p, so numerical convergence is improved by choosing plasma parameters which yield maximum growth at frequencies somewhat, but not substantially, greater than Ω_p. Thus we choose the following representative parameters: $v_A/c = 1.0 \times 10^{-3}$, $\tilde{\beta}_1 = 0.20$, $n_1/n_o = 0.650$, $n_2/n_o = 3.300$, $n_3/n_o = 2.95$, $T_{\|2}/T_1 = 2$, $T_{\|3}/T_1 = 1.4$, $T_e/T_1 = 0.01$, and $T_{\perp 2}/T_{\|2} = T_{\perp 3}/T_{\|3} = 2.0$ so that $T_{\|p}/T_1 = 3.12$.

Figure 1 illustrates the proton velocity distribution corresponding to these parameters. Here $\partial f_p(v_{||},0)/\partial v_{||} < 0$ for all $v_{||} > 0$, whereas $\partial f_p(0,v_\perp)/\partial v_\perp > 0$ for a range of suprathermal perpendicular speeds, indicating the potential for a proton-driven instability. The two-dimensional color representation in Figure 1c shows that, in this model and for these parameters, $f_p(\mathbf{v})$ at $v_{||} \neq 0$ is rather different from the velocity-ring distributions modeled, for example, by *Chen et al.* [2010]. However, because the instability propagates at $k_\perp >> k_{||}$, it is the properties of $f_p(0,v_\perp)$ which are the primary driver of the growing mode, so that we believe our 3-component model of the proton distribution provides a qualitative, if not quantitative, representation of the properties of this instability.

The dispersion properties of the $n = 1$ mode of the proton Bernstein instability in the three-component proton model are very similar to those of the two-Maxwellian model illustrated in Fig. 2 and Fig. 3 of *Gary et al.* [2010] and are not shown here. As is well established, the instability propagates almost, but not exactly, perpendicular to the background magnetic field ($0 < k_{||} << k_\perp$) and near successive harmonics of the proton cyclotron frequency.

Figure 2a displays the wavenumber dependence of γ for the unstable regimes of the first eight unstable Bernstein modes. The angles of propagation correspond to the relative maximum growth rates of the individual harmonics and are as stated in the caption; the frequencies corresponding to the successive growth rate peaks are illustrated in Figure 2c. The perpendicular phase speeds of each unstable cyclotron mode are shown in Figure 2b with the dots representing the phase speed at maximum growth for that mode. For the $\tilde{\beta}_1 = 0.20$ used here, $v_1/v_A = \sqrt{0.10}$, so that the perpendicular phase speed at maximum growth of $\omega_r/k_\perp v_A \simeq 0.74$ is equivalent to $\omega_r/k_\perp v_1 \simeq 2.34$. Thus from Figure 1b, the steep positive slope of the proton perpendicular velocity distribution corresponds to the perpendicular phase speed at maximum growth.

Figure 3 illustrates some linear properties at the relative maximum growth rates of the cyclotron harmonic modes of this instability at $\omega_r \lessapprox 10\Omega_p$ as functions of $\tilde{\beta}_1$ under the condition that all other representative dimensionless parameters stated above are held constant. At constant v_A/c, increases in $\tilde{\beta}_1$ correspond to increases in the temperature of the core proton component. Figure 3a shows that the maximum growth rate of each of these modes lies at $0.10 \leq \tilde{\beta}_1 \leq 0.15$. This is similar to the *Gary et al.* [2010] result from the two-proton-component model which shows a maximum instability growth rate near $\tilde{\beta}_1 \simeq 0.30$. Figure 3b shows the angles of propagation at maximum growth of these harmonics; so increasing $\tilde{\beta}_1$ leads to a monotonic decrease in θ for each mode. Again, this is the same trend as shown in Fig. 3c of *Gary et al.* [2010] with θ decreasing monotonically as $\tilde{\beta}_1$ increases. Figure 3c shows that $\omega_r/k_\perp v_A$ is also a monotonic function of $\tilde{\beta}_1$, with this dimensionless phase speed increasing as the core proton temperature increases. In contrast to the *Gary et al.* [2010] results of $\omega_r/k_\perp v_A \simeq 0.25$, here $\omega_r/k_\perp v_A \simeq 0.60$ near maximum growth rates.

Linear dispersion theory not only provides a relationship between the complex frequency and the wavevector $\mathbf{k}$ for a particular normal mode of the plasma, it also yields dimensionless ratios of quadratic combinations of the various fluctuating field components of that normal mode [e.g., Chapter 5 of *Gary*, 1993]. For the proton Bernstein instability and the range of parameters illustrated in Figure 3, magnetic fluctuations have both a transverse and a compressive component, with $|\delta B_\perp|^2 << |\delta B_{\perp\perp}|^2 \sim |\delta B_{||}|^2$ at maximum growth rate. The corresponding electric field fluctuations are predominantly electrostatic, with $|\delta E_{||}|^2 << |\delta E_{\perp\perp}|^2 << |\delta E_{\perp}|^2$.

For all values of the parameters considered here, $0.96 < |\delta E_{\perp}|^2 < 1.0$; we do not illustrate this result. However, Figure 4 shows two other linear theory quantities which display variations which appear to be characteristic of this instability. Figure 4a illustrates the magnetic compressibility $C_{||}$ [Equation (1)] which is a relatively insensitive function of the cyclotron harmonic number, and, as in the two-component model results of *Gary et al.* [2010], increases with increasing $\tilde{\beta}_1$. Figure 4b shows that, in our three-component proton model, the electric/magnetic field energy ratio [Equation (2)] increases with increasing mode frequency, but is a diminishing function of $\tilde{\beta}_1$; it also approximately satisfies $\sigma_{EE} \sim \omega_r^2$ at $\omega_r >> \Omega_p$.

Figure 5 shows the maximum growth rate and the corresponding electron Landau resonance factor of the $\omega_r \simeq 6\Omega_p$ cyclotron mode of the proton Bernstein instability as functions of T_e/T_1. The γ_m/Ω_p is a decreasing function of the electron/thermal-proton temperature ratio, due to the increasing efficacy of the electron Landau resonance, as indicated by the decreasing magnitude of ζ_e. This indicates that this instability is subject to strong electron Landau damping as the relative electron temperature increases. On the other hand, in the nonresonant limit, the growth rate becomes relatively independent of the electron temperature, suggesting that hybrid simulations, in which electrons are represented as a fluid, may provide an appropriate representation of the nonlinear physics of this instability as long as $T_e/T_1 \lesssim 0.10$.

3. Conclusions

We have carried out numerical solutions of the full kinetic linear dispersion equation for the proton Bernstein instability driven by a proton velocity distribution $f_p(\mathbf{v})$ such that $\partial f_p(v_\perp)/\partial v_\perp > 0$ at suprathermal values of $v_\perp$. We model the proton velocity distribution by means of three components: a Maxwellian represents the relatively cool thermal component, and the difference of two hotter bi-Maxwellians with $T_{\perp j}/T_{\|j} > 1$ represents the velocity-ring-like distributions sometimes observed in in the stormtime magnetosphere. Our results are consistent with previous theoretical results; the instability propagates almost perpendicular to $\mathbf{B}_o$ with relative maxima near successive harmonics of the proton cyclotron frequency. The fluctuating electric fields are essentially electrostatic, and the fluctuating magnetic fields have both compressive ($\delta B_{\|}$) and transverse ($\delta B_{\perp\perp}$) components. The primary new results presented here are for scalings of the maximum growth rate of the proton Bernstein instability driven by a suprathermal velocity ring distribution. In our model the maximum growth rate is found in the range $0.10 < \tilde{\beta}_1 < 0.15$ and at perpendicular phase speeds $\omega_r/k_\perp v_A \simeq 0.6$. As $\tilde{\beta}_1$ increases, the angle of instability propagation moves away from the direction perpendicular to the background magnetic field, and the magnetic compressibility increases. The maximum instability growth rate is a monotonically decreasing function of the electron/thermal-proton temperature ratio.

The primary value of the results presented here are that they are exact; our calculations represent full solutions of the kinetic linear theory dispersion equation, with no approximations concerning the magnitudes of the dimensionless frequencies, wavevectors or plasma parameters. The primary limitations of this work are two. First, our calculations strictly apply only to homogeneous plasmas and should include consequences of propagation in the inhomogeneous geomagnetic field to increase their magnetospheric relevance. Second, although our model represents the positive slope of the $f_p(0, v_\perp)$ which drives the proton Bernstein instability, it does not fully represent the $v_\parallel \neq 0$ properties of stormtime proton velocity distributions predicted by the RAM model as in *Chen et al.* [2010].

Acknowledgments. This work was performed under the auspices of the U.S. Department of Energy (DOE). It was supported primarily by the Defense Threat Reduction agency under the "Basic Research for Combating Weapons of Mass Destruction (WMD)" Program, projects IACRO 10-4946I and IACRO 10-4284I. Further support has been provided by the Dynamic Radiation Environment Assimiliation Model (DREAM) Project at Los Alamos National Laboratory.

References

Akimoto, K., K. Papadopoulos, and D. Winske (1985), Lower-hybrid instabilities driven by an ion velocity ring, *J. Plasma Phys.*, *34*, 445.

Ashour-Abdalla, M., J. N. Leboeuf, D. Schriver, J.-M. Bosqued, N. Cornilleau-Wehrlin, V. Sotnikov, A. Marcaudon, and A. N. Fazakerley (2006), Instabilities driven by ion shell distributions observed by Cluster in the midaltitude plasma sheet boundary layer, *J. Geophys. Res., 111*, A10223.

Boardsen, S. A., D. L. Gallagher, D. A. Gurnett, W. K. Peterson, and J. L. Green (1992), Funnel-shaped, low-frequency equatorial waves, *J. Geophys. Res., 97*, 14,967.

Borovsky, J. E., and M. H. Denton (2009), Relativistic-electron dropouts and recovery: A superposed epoch study of the magnetosphere and the solar wind, *J. Geophys. Res., 114*, A02201, doi: 10.1029/2008JA013128.

Bortnik, J., and R. M. Thorne (2010), Transit time scattering of energetic electrons due to equatorially confined magnetosonic waves, *J. Geophys. Res., 115*, A07213.

Chen, L., R. M. Thorne, V. K. Jordanova, C.-P. Wang, M. Gkioulidou, L. Lyons, and R. B. Horne (2010), Global simulation of EMIC wave excitation during the 21 April 2001 storm from coupled RCM-RAM-HOTRAY modeling, *J. Geophys. Res., 115*, A07209.

Chen, L., R. M. Thorne, V. K. Jordanova, M. F. Thomsen, and R. B. Horne (2011), Magnetosonic wave instability analysis for proton ring distributions observed by the LANL MPA detector, *J. Geophys. Res., 116* in press.

Dendy, R. O., and K. G. McClements (1993), Ion cyclotron wave emission at the quasi-perpendicular bow shock, *J. Geophys. Res., 98*, 15,531.

Denton, R. E., M. J. Engebretson, A. Keiling, A. P. Walsh, S. P. Gary, P. M. E. Décréau, C. A. Cattell, and H. Réme (2010), Multiple harmonic ULF waves in the plasma sheet boundary layer: Instability analysis, *J. Geophys. Res., 115*, A12224, doi:10.1029/2010JA015928.

Gary, S. P. (1993), *Theory of Space Plasma Instabilities*, Cambridge University Press.

Gary, S. P., K. Liu, D. Winske, and R. E. Denton (2010), Ion Bernstein instability in the terrestrial magnetosphere: Linear dispersion theory, *J. Geophys. Res., 115*, A12209, doi:10.1029/2010JA015965.

Gul'elmi, A. V., B. I. Klaine, and A. S. Potapov (1975), Excitation of magnetosonic waves with discrete spectrum in the equatorial vicinity of the plasmapause, *Planet. Space Sci.*, *23*, 279.

Horne, R. B., G. V. Wheeler, and H. St. C. K. Alleyne (2000), Proton and electron heating by radially propagating fast magnetosonic waves, *J. Geophys. Res., 105*, 27,597.

Horne, R. B., R. M. Thorne, S. A. Glauert, N. P. Meredith, D. Pokhotelov, and O. Santolík (2007), Electron acceleration in the Van Allen radiation belts by fast magnetosonic waves, *Geophys. Res. Lett., 34*, L17107.

Janhunen, P., A. Olsson, A. Vaivads, and W. K. Peterson (2003), Generation of Bernstein waves by ion shell distributions in the auroral region, *Ann. Geophys.*, *21*, 881.

Jordanova, V. K., J. U. Kozyra, A. F. Nagy, and G. V. Khazanov (1997), Kinetic model of the ring current-atmosphere interactions, *J. Geophys. Res., 102*, 14,279.

Lee, J. K., and C. K. Birdsall (1979), Velocity space ring-plasma instability, magnetized, Part II: Simulation, *Phys. Fluids*, *22*, 1315.

Liu, K., S. P. Gary, and D. Winske (2011), Excitation of magnetosonic waves in the terrestrial magnetosphere: Particle-in-cell simulations, *J. Geophys. Res.,* submitted.

McClements, K. G., and R. O. Dendy (1993), Ion cyclotron harmonic wave generation by ring protons in space plasmas, *J. Geophys. Res., 98*, 11,689.

McClements, K. G., R. O. Dendy, and C. N. Lashmore-Davies (1994), A model for the generation of obliquely propagating ULF waves near the magnetic equator, *J. Geophys. Res., 99*, 23,685.

Meredith, N. P., R. B. Horne, and R. R. Anderson (2008), Survey of magnetosonic waves and proton ring distributions in the Earth's inner magnetosphere, *J. Geophys. Res., 113*, A06213.

Meredith, N. P., R. B. Horne, S. A. Glauert, D. N. Baker, S. G. Kanekal, and J. M. Albert (2009), Relativistic electron loss timescales in the slot region, *J. Geophys. Res., 114*, A03222.

Ni, B., and D. Summers (2010), Resonance zones for electron interaction with plasma waves in the Earth's dipole magnetosphere. II. Evaluation for oblique chorus, hiss, electromagnetic ion cyclotron waves, and magnetosonic waves, *Phys. Plasmas*, *17*, 042903.

Perraut, S., A. Roux, P. Robert, R. Gendrin, J.-A. Sauvaud, J.-M. Bosqued, G. Kremser, and A. Korth (1982), A systematic study of ULF waves above F_{H+} from GEOS 1 and 2 measurements and their relationships with proton ring distributions, *J. Geophys. Res.*, *87*, 6219.

Pokhotelov, D., F. Feveuvre, R. B. Horne, and N. Cornilleau-Wehrlin (2008), Survey of ELF-VLF plasma waves in outer radiation belt observed by Cluster STAFF-SA experiment, *Ann. Geophys.*, *26*, 3269.

Roth, I., and M. K. Hudson (1985), Lower hybrid heating of ionospheric ions due to ion ring distributions in the cusp, *J. Geophys. Res.*, *90*, 4191.

Russell, C. T., R. E. Holzer, and E. J. Smith (1970), OGO 3 observations of ELF noise in the magnetosphere 2. The nature of equatorial noise, *J. Geophys. Res.*, *75*, 755.

Santolík, O., J. S. Pickett, D. A. Gurnett, M. Maksimovic, and N. Cornilleau-Wehrlin (2002), Spatiotemporal variability and propagation of equatorial noise observed by Cluster, *J. Geophys. Res.*, *107*, 1495.

Santolík, O., F. Nemec, K. Cereová, E. Macúsova, Y. de Conchy, and N. Cornilleau-Wehrlin (2004), Systematic analysis of equatorial noise below the lower hybrid frequency, *Ann. Geophys.*, *22*, 2587.

Shprits, Y. Y. (2009), Potential waves for pitch-angle scattering of near-equatorially mirroring energetic electrons due to the violation of the second adiabatic invariant, *Geophys. Res. Lett.*, *36*, L12106.

Tao, X., J. M. Albert, and A. A. Chan (2009), Numerical modeling of multidimensional diffusion in the radiation belts using layer methods, *J. Geophys. Res., 114*, A02215.

Figure 1. The proton velocity distribution in arbitrary units in the three-component model using the representative plasma parameters stated in Section 2. (a) The parallel velocity distribution $f_p(v_{\|}, 0)$, (b) the perpendicular velocity distribution $f_p(0, v_{\perp})$, and (c) the two-dimensional distribution $f_p(v_{\|}, v_{\perp})$.

Figure 2. Linear theory properties of the first eight cyclotron modes of the proton Bernstein instability for the representative parameters stated in Section 2. (a) Growth rates of the modes as functions of the wavenumber. (b) Perpendicular phase speed $(\omega_r/k_{\perp}v_A)$ of the modes as functions of the wavenumber. The dots on each curve here correspond to the wavenumber of maximum growth for each cyclotron mode. (c) Growth rates of the modes as functions of the real frequency. Here each curve is plotted for a fixed value of θ corresponding to the maximum growth rate of that cyclotron mode. These angles of propagation are, starting with the $\omega_r \simeq 3\Omega_p$ mode, $\theta = 81.40^o$, 83.25^o, 84.45^o, 85.30^o, 85.90^o, 86.35^o, 86.75^o, and 87.00^o.

Figure 3. Linear theory properties of the first eight cyclotron modes of the proton Bernstein instability as functions of the real frequency ω_r. Here each symbol corresponds to a maximum growth rate of the individual cylotron harmonic modes illustrated in Figure 2 at six different values of $\tilde{\beta}_1$ as labeled in panel (a); all other parameters have the representative values stated in Section 2. (a) Maximum growth rate, (b) propagation angle at maximum growth rate, and (c) dimensionless perpendicular phase speed $\omega_r/k_{\perp}v_A$.

Figure 4. Linear theory properties of the first eight cyclotron modes of the proton Bernstein instability as functions of the real frequency ω_r. Here each symbol corresponds to a maximum growth rate of the individual cylotron harmonic modes illustrated in Figure 2 at six different values of $\tilde{\beta}_1$ as labeled in panel (a); all other parameters have the representative values stated in Section 2. (a) Magnetic compressibility $C_{\|}$ and (b) the electric/magnetic field energy ratio σ_{EE}.

Figure 5. The maximum growth rate (solid line) and corresponding electron Landau resonance factor $\zeta_e \equiv \omega_r/\sqrt{2}k_{\|}v_e$ (dashed line) of the $\omega_r \simeq 6\Omega_p$ cyclotron mode of the proton Bernstein instability as functions of T_e/T_1. All other parameters have the representative values stated in Section 2. The wave parameters corresponding to this maximum growth are $kv_1/\Omega_p \simeq 2.57$, $\theta \simeq 85.4^o$, and $\omega_r/\Omega_p \simeq 5.95$ and are relatively independent of T_e/T_1 here.

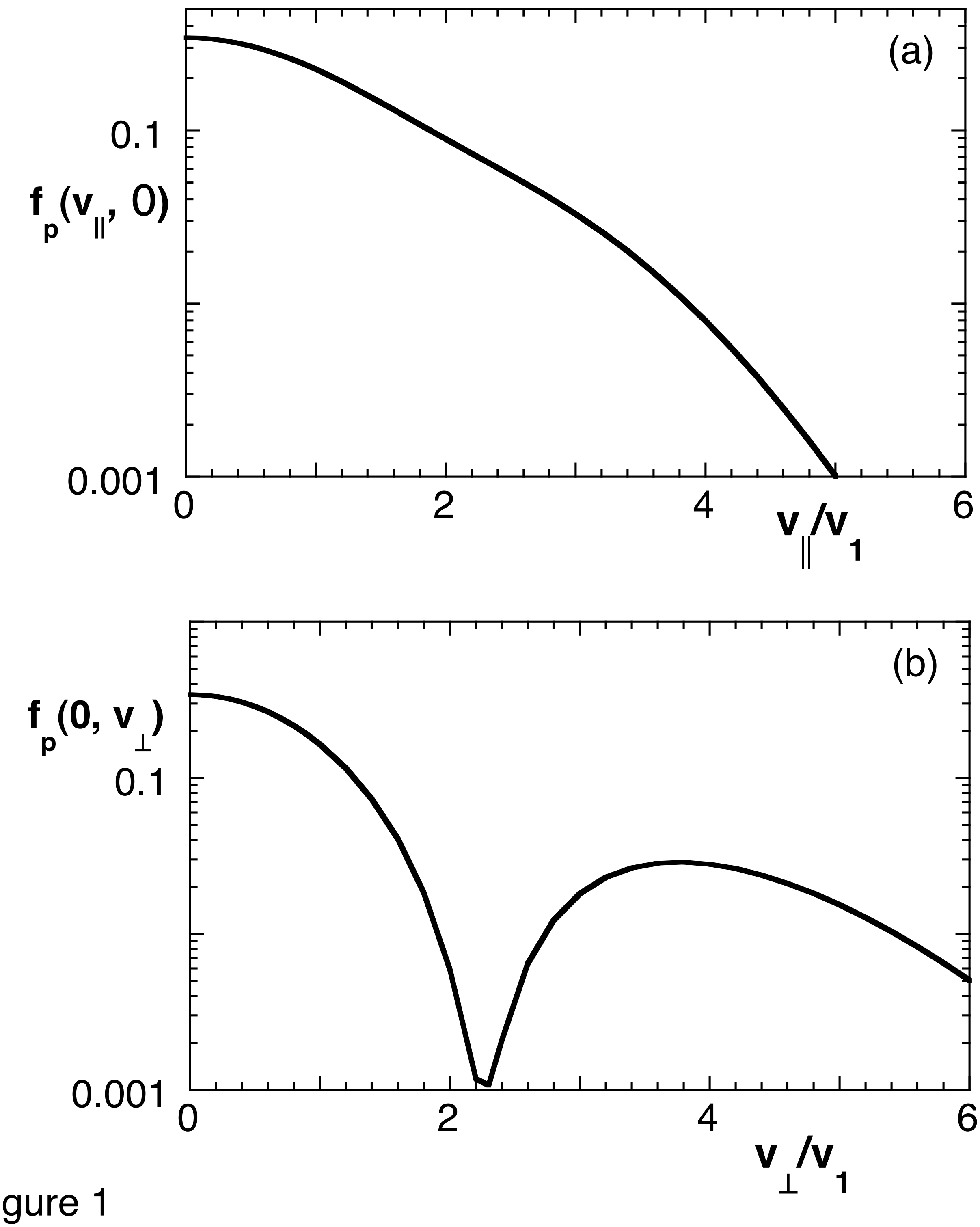

Figure 1

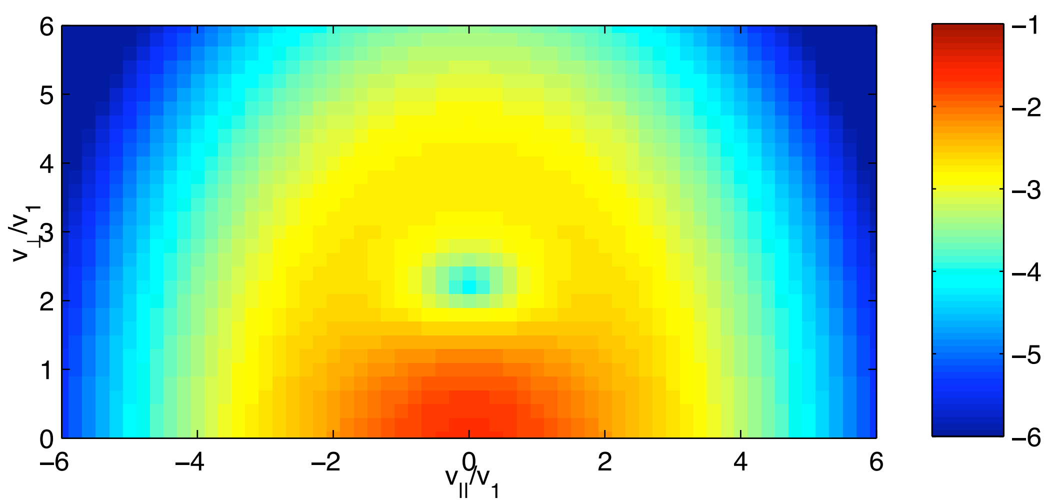

6
5
4
3
2
1
0
v⊥/v1
−6
−4
−2
0
2
4
6
v||/v1
−1
−2
−3
−4
−5
−6

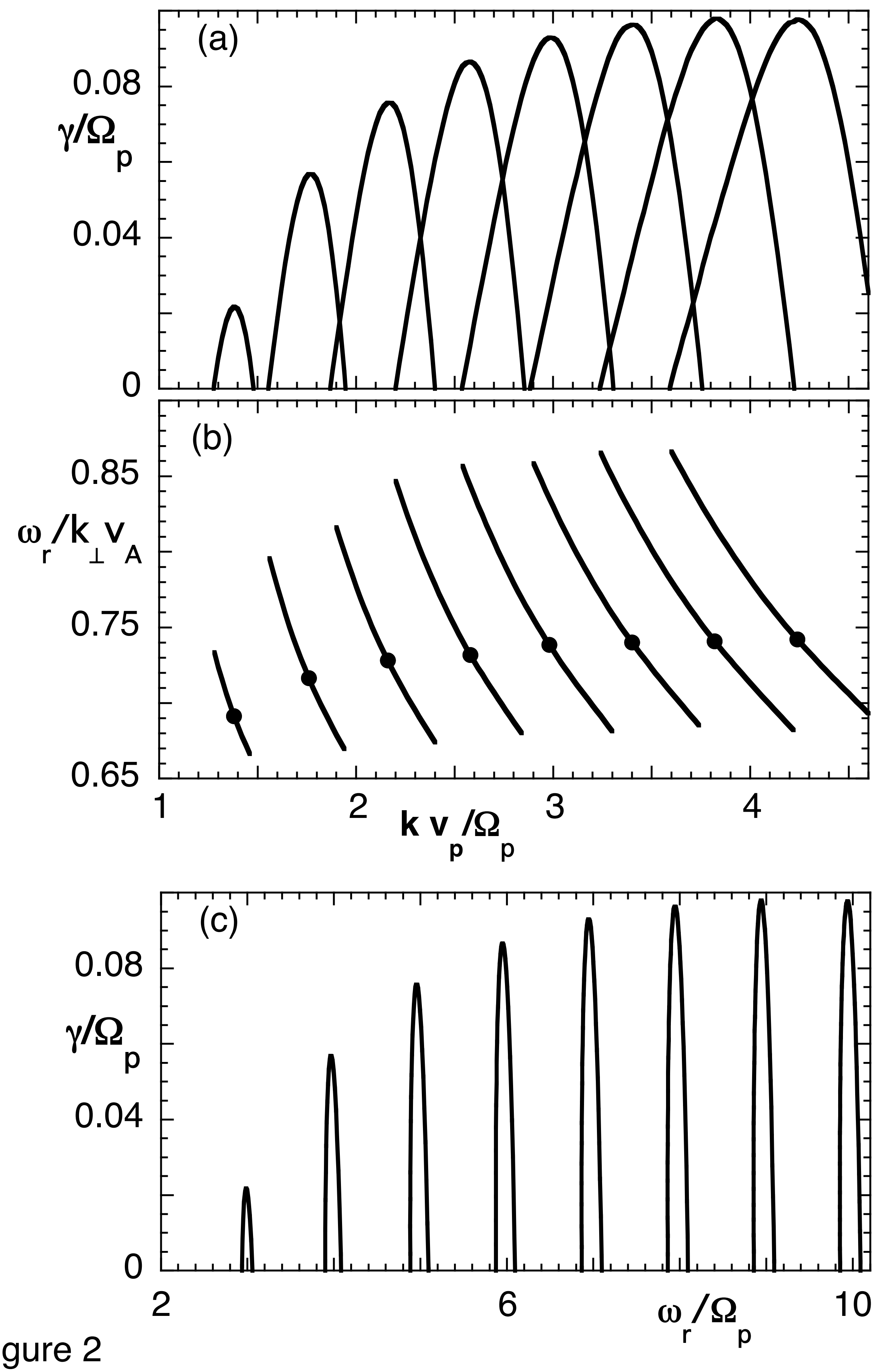
(a)
0.08
γ/Ω_p
0.04
0
(b)
0.85
ω_r/k_⊥v_A
0.75
0.65
1
2
3
4
k v_p/Ω_p
(c)
0.08
γ/Ω_p
0.04
0
2
6
ω_r/Ω_p
10

Figure 2

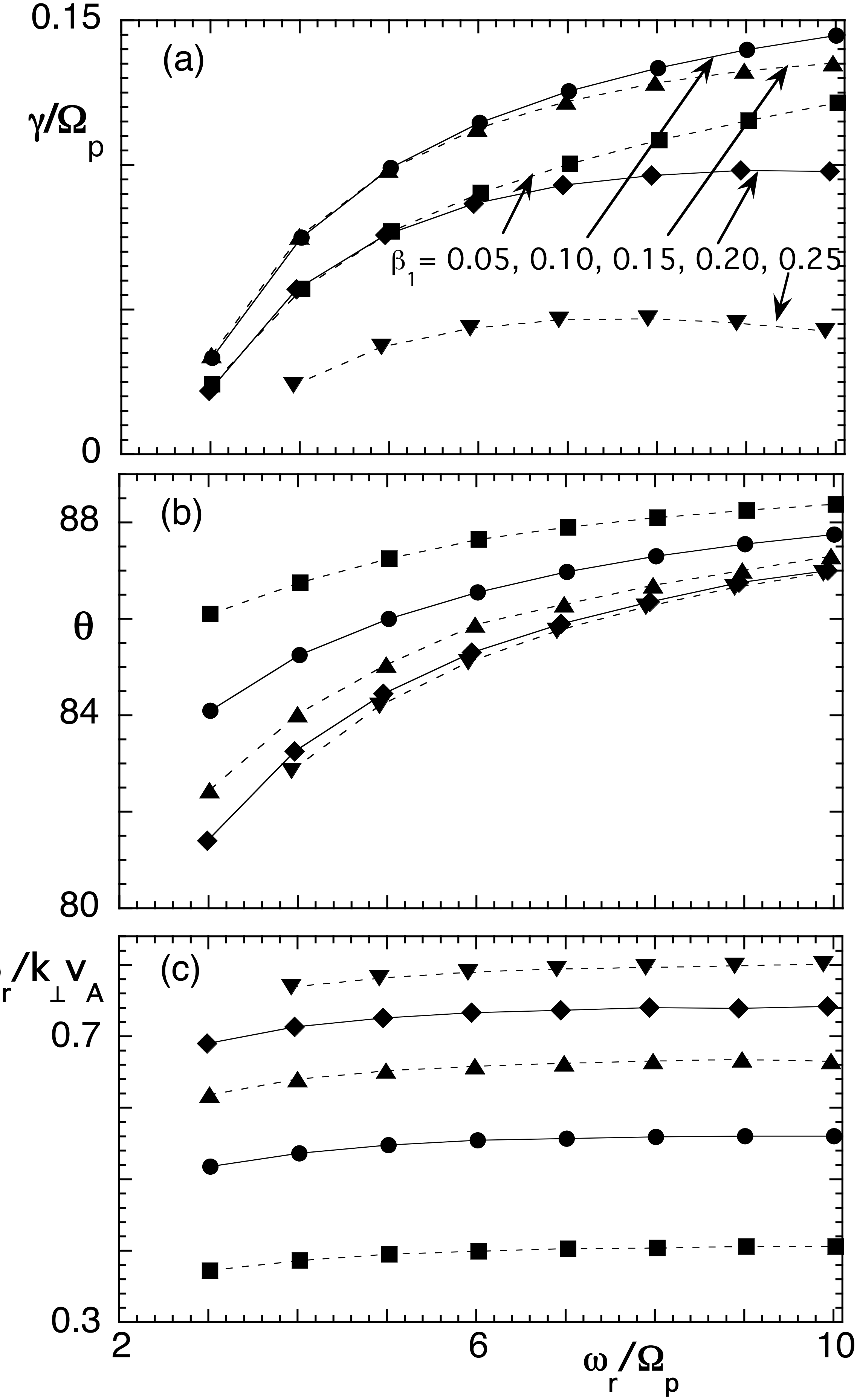

0.15
(a)
γ/Ω_p
β_1 = 0.05, 0.10, 0.15, 0.20, 0.25
0
(b)
88
θ
84
80
(c)
ω_r/k_⊥v_A
0.7
0.3
2
6
10
ω_r/Ω_p

Figure 3

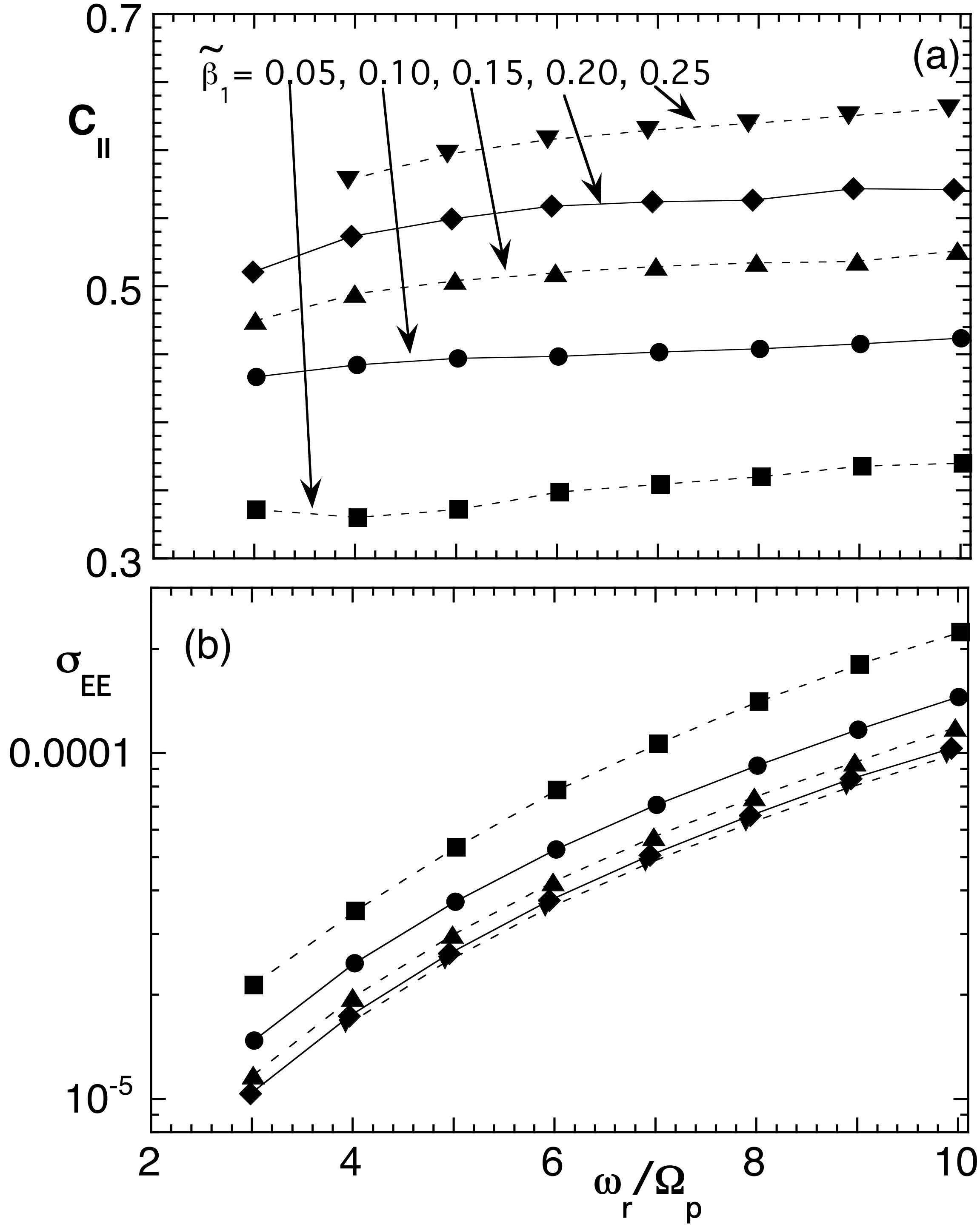

0.7
0.5
0.3
C_II
(a)
$\tilde{\beta}_1$= 0.05, 0.10, 0.15, 0.20, 0.25
(b)
σ_EE
0.0001
10^-5
2
4
6
8
10
ω_r/Ω_p

Figure 4

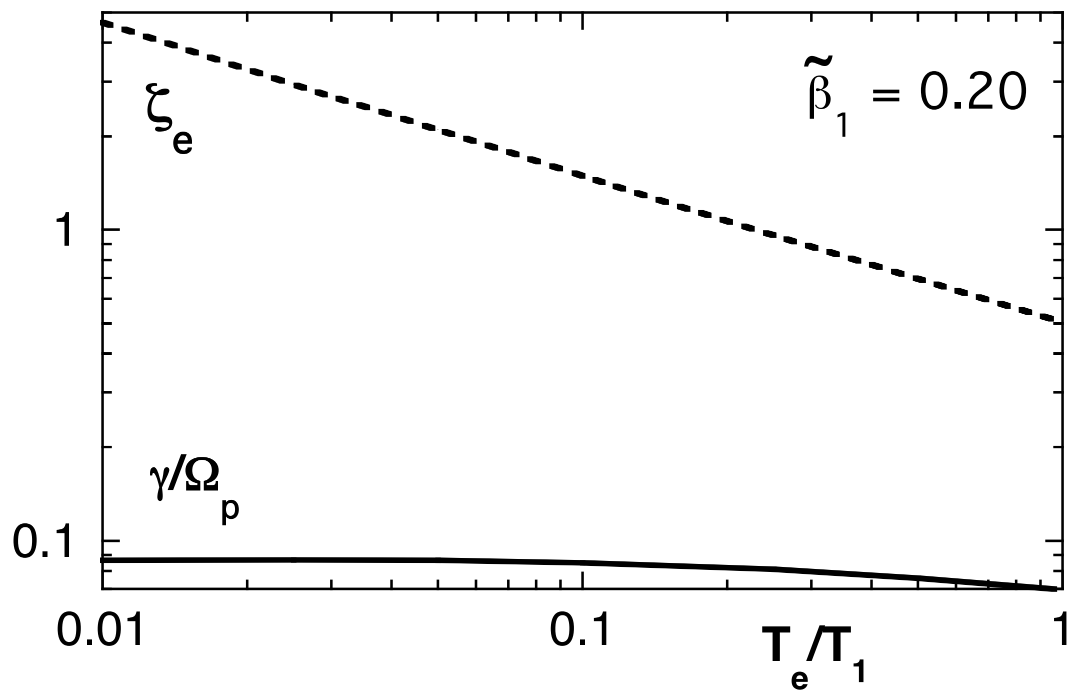

Figure 5